

Ferroelectric higher-order topological insulator in two dimensions

Ning Mao,¹ Runhan Li,¹ Xiaorong Zou,¹ Ying Dai,^{1,*} Baibiao Huang,¹ and Chengwang Niu^{1,†}

¹*School of Physics, State Key Laboratory of Crystal Materials, Shandong University, Jinan 250100, China*

The interplay between ferroelectricity and band topology can give rise to a wide range of both fundamental and applied research. Here, we map out the emergence of nontrivial corner states in two-dimensional ferroelectrics, and remarkably demonstrate that ferroelectricity and corner states are coupled together by crystallographic symmetry to realize the electric control of higher-order topology. Implemented by density functional theory, we identify a series of experimentally synthesized two-dimensional ferroelectrics, such as In_2Se_3 , BN bilayers, and SnS , as realistic material candidates for the proposed ferroelectric higher-order topological insulators. Our work not only sheds new light on traditional ferroelectric materials but also opens an avenue to bridge the higher-order topology and ferroelectricity that provides a nonvolatile handle to manipulate the topology in next-generation electronic devices.

Time-reversal polarization, defined as the differences between Wannier charge centers of Kramers pair, plays a pivotal role in the \mathbb{Z}_2 classification of electronic topological insulators (TIs) [1–3]. Armed with topologically protected metallic boundary (surface or edge) states, TIs ensure the dissipationless nature of spin transport with promising applications in spintronics [4–7]. The existence of boundary-localized mass domains, as generally accepted, will open up a boundary band gap, thereby trivializing the time-reversal polarization in TIs. Remarkably, recent investigations proposed that the hinge or corner states may appear, resulting in the intriguing quantum phase named higher-order TIs (HOTIs) [8–12]. For which, n th-order HOTIs in d dimensions host symmetry protected features not at the $(d - 1)$ -dimensional but at $(d - n)$ -dimensional boundaries. In particular, as the expectation value of position operator for Wannier functions, the quantized polarization can be topological indices for C_n -symmetric HOTIs, which form into \mathbb{Z}_2 , $\mathbb{Z}_2 \times \mathbb{Z}_2$, or \mathbb{Z}_3 indexes [13–15]. As a novel extension of TIs, theoretical models and material candidates of HOTIs have been proposed both in two/three dimensions [16–24], and remarkably been experimentally observed in three-dimensional Bi [25], WTe_2 [26], and Bi_4Br_4 [27]. However, for two-dimensional electronic materials, the experimental confirmation of HOTIs has been elusive so far.

On the other hand, polarization has received great attention in ferroelectric materials [28–39]. One important characteristic of the ferroelectric materials is the existence of two degenerate structures with opposite polarization that could be switched by an external electric field [40]. In fact, the switchable electric polarization, when coupled to other properties such as ferromagnetism, ferroelasticity, valley, skyrmion, spin polarization, and/or nontrivial band topology, provides a nonvolatile control with the implementation of gate voltages [41–48]. Moreover, the separation of the center of positive and negative electric charge in ferroelectric systems is currently served as a hallmark of obstructed atomic limits (OALs) within the framework of topological quantum chemistry theory [49, 50]. The OALs have recently attracted significant in-

terest, since they could manifest themselves at the boundary in terms of metallic surface/edge states, regardless of spin-orbit coupling (SOC) or bulk band inversion [51–56]. Even more, some of them could host hinge/corner states as a result of filling anomaly, which leads to the higher-order topology. Therefore, a natural question arises as to whether the ferroelectric polarization can result in the emergence of HOTIs, especially in two dimensions.

In the present work, we demonstrate the emergence of higher-order topological phases in 2D ferroelectrics including both the in-plane and out-of-plane ferroelectricity. Moreover, we reveal that the in-plane polarizations, which can enforce the non-quantized ones and the quantized ones, endow the emergence of the corner states and even may serve as the topological invariants. Effective models for both the quantized and non-quantized in-plane polarizations are constructed to demonstrate the feasibility of attaining the proposed 2D ferroelectric HOTIs. Remarkably, based on the first-principles calculations, a wide range of 2D ferroelectrics are testified to possess fractional corner charges, resulting in higher-order topological phases. For which, the implementing of an external electric field could switch the directions of ferroelectric polarization and in turn change the position of corner states and/or mediates the topological phase transitions. Our results indicate that 2D ferroelectric materials provide an up-and-coming platform to achieve and control higher-order corner states with experimentally feasible examples.

It has long been known that polarization is closely related to the position of the Wannier function, which can be transformed into the Berry phase of the occupied bands as

$$\mathbf{P} = P^{occ} \hat{x} P^{occ} = -\frac{1}{2\pi} \int_k^{k+2\pi} \text{Tr} [\mathcal{A}_k] dk, \quad (1)$$

where P^{occ} and \hat{x} are the projection and position operators, respectively. \mathcal{A}_k is the gauge-dependent Berry connection in terms of $[\mathcal{A}_k]^{mn} = -i \langle u_k^m | \partial_k | u_k^n \rangle$, and its integral along a closed path is called as Berry phase. The direction of polarization is determined by the displacement of Wannier function, and the polarization can be quantized or non-quantized limited by the crystal symmetry. Remarkably, as we demonstrate below, an in-plane polarization, no matter quantized or non-quantized, would give rise to the two-dimensional higher-order corner states.

* daiy60@sdu.edu.cn

† c.niu@sdu.edu.cn

We consider first the quantized polarization in a two-band tight-binding model on a honeycomb lattice

$$H = \sum_i \lambda_i c_i^\dagger c_i + t_1 \sum_{\langle ij \rangle} c_i^\dagger c_j + t_2 \sum_{\langle\langle ij \rangle\rangle} c_i^\dagger c_j + t_3 \sum_{\langle\langle\langle ij \rangle\rangle\rangle} c_i^\dagger c_j. \quad (2)$$

The first term is the sublattice potential, which is needed for the broken of inversion symmetry (\mathcal{I}). The second, third, and fourth terms represent the nearest, next-nearest, and next-next-nearest neighbor hoppings, as depicted in Fig. 1(a). In Fig. 1(b), we show the band structures of the Hamiltonian under the OAL phase. Indeed, the moving of Wannier charge centers leads to a quantized polarization as shown by Fig. 1(c). However, the sum of the polarization, bounded by C_3 symmetry, can necessarily be zero in the bulk due to $\mathbf{P}_{\text{bulk}} = \sum_i (\mathbf{P}_i + C_3 \mathbf{P}_i + C_3^{-1} \mathbf{P}_i) = 0$, while ones at the edges and corners cannot be offsetted as displayed in Fig. 1(a), leading to the non-vanished polarization as $\mathbf{P}_{\text{edge}} = \sum_i (\mathbf{P}_i + C_3 \mathbf{P}_i)$ and $\mathbf{P}_{\text{corner}} = \sum_i \mathbf{P}_i$. Hence electrons from the bulk will be driven to the edges and corners, forming the edge and corner states. Figure 1(d) presents the energy level of a finite triangular flake. Clearly, the edge and corner states emerge near the Fermi level, and the energy level of edge states is lower than corner states caused by the difference of polarization in the edge and corner. Moreover, corner states originated from the valence and conduction bands are degenerated in energy, giving rise to a phenomenon of filling anomaly. In that sense, the corner states can be pushed into the conduction or valence bands as a whole, and the positive or negative charge will be generated to affect the charge neutrality.

For a better control of the corner states, the non-quantized polarization has to be introduced by breaking the C_6 , C_4 , and C_3 symmetries. To study systematically the switchable corner states, we then focus on a simple model of one atom located at the center of a 2D square lattice [16], and the Hamiltonian can be expressed as

$$H_0 = [(m - t(\cos k_x + \cos k_y))\tau_z - \lambda(\sin k_x \sigma_x + \sin k_y \sigma_y)]\tau_x, \quad (3)$$

where m sets the energy offset between s and p orbitals. Spin-orbit coupling (SOC) termed with λ induces their hybridization while the nearest-neighbor hopping (t) bridges the relations for $s-s$ or $p-p$ orbitals. After diagonalizing the Hamiltonian and considering the zero-energy conditions for four high symmetry points of Γ , X, Y, and M, the nontrivial TIs are expected to emerge as $|m/t| < 2$ (See Fig. S1 [57]). The non-quantized polarization affects the electric potential of the system and causes a potential imbalance for the overall system. In this sense, we add an electric potential term to mimic the non-quantized polarization

$$H_E = \sum_i c_i^\dagger [eF(x \cos \theta + y \sin \theta)] c_i, \quad (4)$$

where $c_i^\dagger = (c_{i\uparrow}^\dagger, c_{i\downarrow}^\dagger)$ are electron creation operators at the site i . Besides the elementary charge e , H_E is expressed with the amplitude given by F and orientation defined by θ . It is clear

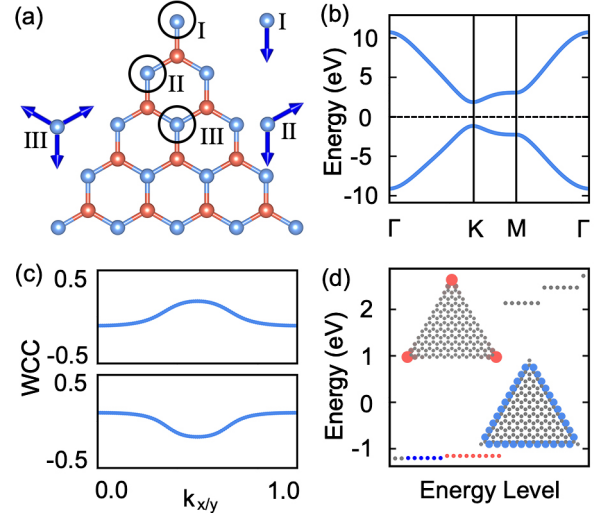


FIG. 1. (a) Sketch of the finite triangular lattice with C_3 symmetry. The quantized polarization in the bulk (III) can always be annihilated, whereas the edge (II) and corner (I) may possess uncompensated polarization. (b) Band structures of the two-band Hamiltonian, and the Fermi level is indicated with a dashed line. The parameters are set as $\lambda_1 = 2$, $\lambda_2 = -1$, $t_1 = -3$, $t_2 = 0.1$, and $t_3 = -0.2$, respectively. (c) The Wilson bands of the occupied band along k_x (up) and k_y (down) directions. (d) Energy spectrum of the finite nanoflake. The red dots near the Fermi level represent the in-gap corner states, and the blue ones denote the edge states. The distributions of corner and edge states are plotted in the inset.

that, under an in-plane electric potential along \hat{y} direction, \mathcal{I} , C_6 , C_4 , C_3 , and C_{2x} symmetries are broken, and remarkably, as illustrated in Fig. S1 [57], one can find that the corner states appear, serving as a direct signal of HOTI.

However, the in-gap corner states appear only at specific corners, inspiring us to understand their physical origin. It is well known that electrons will acquire a transverse velocity in the presence of the in-plane electric fields, as schematically shown in Fig. 2(a). This may lead to corner charge accumulation and thus manifest the corner states protected by the rotation symmetry. To map out the role of rotation symmetry and polarization, we choose four representatives with different in-plane orientations, where the rotation symmetries are highly sensitive to the orientations. In the absence of electric potential, the considered square lattice has both $C_{2x} = -i\sigma_x$ and $C_{2y} = -i\sigma_y$, but no polarization and then no corner states [see Fig. S1 [57]]. If an electric potential is perpendicular to the $\hat{x}(\hat{y})$ -direction, $C_{2y}(C_{2x})$ will be broken, and otherwise it will be conserved. For example in Fig. 2(b), C_{2y} is broken, while C_{2x} survives and ensures the existence of corner states. Interestingly, the in-gap corner states can be tuned into opposite corners when the in-plane electric field as well as the polarization is reversed as shown in Fig. 2(e). Similar results with corner states localized on C_{2y} -symmetric positions are shown in Figs. 2(c) and 2(d). Therefore, one can realize the nonvolatile control of the corner states.

Material candidates. Having demonstrated the interplay of

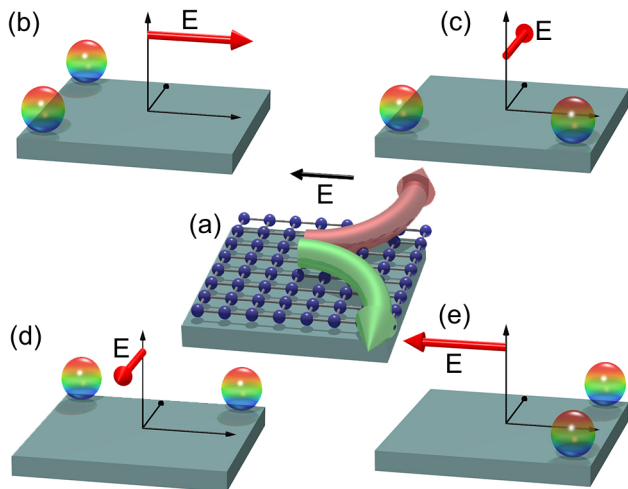


FIG. 2. (a) In-plane polarization and (b)-(e), corner states under the in-plane electric field. A transverse current is generated under in-plane electric field, which leads to the in-plane polarization and then the birth of corner states in symmetric corners. Corner states are indicated with rainbow balls and arrows denote the directions of the in-plane electric field.

HOTIs and polarization, we aim now at its realization in electronic materials, where remarkably the in-plane polarization \mathbf{P} can be defined by

$$\mathbf{P} = p_1 \mathbf{a}_1 + p_2 \mathbf{a}_2. \quad (5)$$

Here, \mathbf{a}_1 and \mathbf{a}_2 are primitive lattice vectors, and the components p_1 and p_2 can be served as the topological indices that are equivalent to the quantized Berry phase [58]. The 2D ferroelectric materials lack the \mathcal{T} intrinsically and hence usually possess the electric polarization, revealing the great opportunities for HOTIs in 2D ferroelectric materials. In addition, the ferroelectricity nature has been demonstrated experimentally in abundant 2D layered materials, and indeed the ferroelectric switching is currently maturing into a significant burgeoning research, therefore, it would be of great significance to make a bridge between HOTIs and 2D ferroelectricity.

In_2Se_3 is one of the most famous examples of 2D ferroelectric materials, which has been widely explored with promising applications in phase-change memory, thermoelectric, photoelectric, and catalysis [59–63]. The monolayer is stacking with a sequence of Se1-In1-Se2-In2-Se1 that can be easily realized by physical exfoliation and/or chemical vapor deposition. The ZB' and WZ' phases of In_2Se_3 , as shown in Fig. 3(a), are the degenerate ground states that have already been synthesized [64–66]. They belong to space group $P3m1$ (No.156). For ZB' phase, three Se atoms occupy two 1a and one 1c Wyckoff positions, whereas two In atoms occupy 1b and 1c Wyckoff positions. While three Se atoms occupy 1a, 1b, and 1c Wyckoff positions, and two In atoms occupy 1a and 1c Wyckoff positions for WZ' phase.

According to the Wilson loop calculations as illustrated in Fig. 3(b), the electron transfer occurs when atoms are brought together to form the crystal of In_2Se_3 , i.e., the electrons of

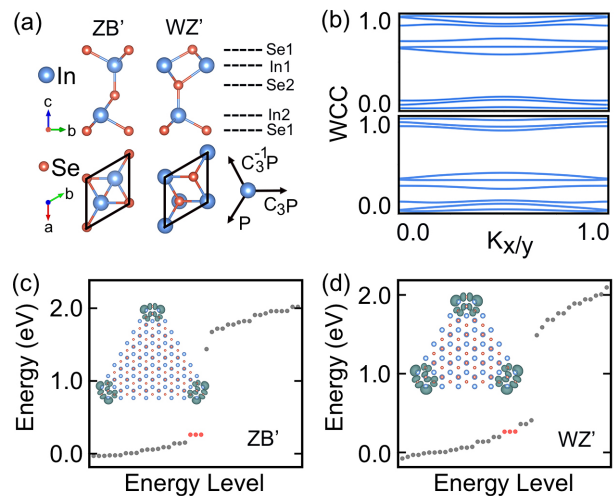


FIG. 3. (a) Top and side views of In_2Se_3 in ZB' and WZ' phases. (b) Wilson bands of the occupied bands along k_x (up) and k_y (down) directions. Energy spectrum of In_2Se_3 in (c) ZB' and (d) WZ' phases. The red dots near the Fermi level represent the in-gap corner states. Distributions of corner states are displayed in the insets.

In move to Se, giving rise to the in-plane electric polarization. Limited by C_3 symmetry, the polarization induced by the electron distribution between In1/In2 and Se2 atoms can be quantized as

$$\mathbf{P} = (1/3, 1/3). \quad (6)$$

Although such a quantized polarization can be annihilated in the bulk as shown in Fig. 3(a), the uncompensated polarization remains intact at the corners, which renders the emergence of fractional charge with $2e/3$ on the corners of C_3 -symmetric finite lattice, and yields the coexistence of 2D ferroelectricity and higher-order topology, namely 2D ferroelectric HOTIs. To further identify the nature of HOTIs, we construct a triangular nanoflake of In_2Se_3 , which preserves the C_3 symmetry for both the bulk and edge. As plotted in Figs. 3(c) and 3(d), three degenerate in-gap states arise around the Fermi level, accumulating in three corners of Se2 atoms. However, the emergence of corner states between ZB' and WZ' phases are nearly the same, rendering a difficulty to control the corner states by an external electric field.

Aiming at revealing the nonvolatile control of corner states and the universality of pronounced ferroelectric HOTIs, we turn to the currently proposed sliding ferroelectricity, which remarkably reveals a universal approach and enables the design of 2D ferroelectric materials out of inherent polar compounds [29, 30, 67, 68]. To date, such a theory has been successfully applied to a bunch of 2D binary compounds XY and transition-metal dichalcogenides XY_2 , such as BN, ZnO, AlN, GaN, SiC, InSe, GaSe, WTe_2 , MoS_2 , VS_2 , and so on [69]. In fact, all of these XY and XY_2 are C_3 -symmetric polar materials, where the electrons transfer from X to Y . Therefore, a large quantized in-plane polarization is generated and drives the Coulomb interaction. If the bilayer lose mirror symmetry (\mathcal{M}_z) perpendicular to the z -axis, the Coulomb

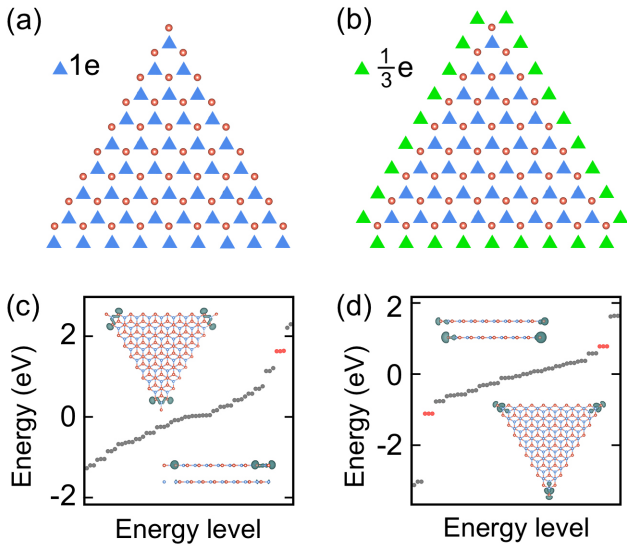


FIG. 4. (a) Finite nanoflake with atoms at positions of red circles. Limited by the polarization, electrons of red circles move to positions of blue triangles, which is C_3 -symmetric in the bulk but not in the corner. (b) Finite nanoflake formed by distributing the edge electrons shown in a, averagely in three edges. This configuration restores the C_3 symmetry in the corner, and leads to the $2e/3$ corner charges. Energy spectrums of finite nanoflake for BN bilayer in (c) AB stacking and (d) BA stacking. Red dots represent the in-gap corner states, and the distributions of corner states are plotted in the insets.

interaction will introduce a non-quantized out-of-plane polarization, making the systems to be the out-of-plane ferroelectric materials that can be controlled by the external electric field.

We take boron nitride (BN) as an example. The valence atomic configurations for B and N atoms located at 1d and 1f Wyckoff position are $2s_22p_1$ and $2s_22p_3$, respectively, and when forming into the BN compound, all valence electrons of B are moved to the position of N, giving rise to the in-plane electric polarization along the B-N bond as

$$\mathbf{P} = (2/3, 1/3). \quad (7)$$

When considering only the polarization, the Wannier centers move from B atoms to the position of N atoms, leading to a neutral and integer charge configuration as schematically shown in Fig. 4(a). However, such a configuration is not C_3 -symmetric at corners. To preserve the symmetry, all of the Wannier centers have to be equally distributed over the three sectors, leaving the edge charges in multiples of $e/3$ as illustrated in Fig. 4(b). Moreover, each corner is related to two fractional Wannier centers and thus manifests the corner charges of $2e/3$.

To explicitly testify the existence of fractional corner charges, triangular nanoflakes of BN bilayers are constructed. Figures 4(c) and 4D display the energy spectrum and distributions of corner states for the AB and BA stackings with sliding ferroelectricity, respectively. The bulk energy gaps

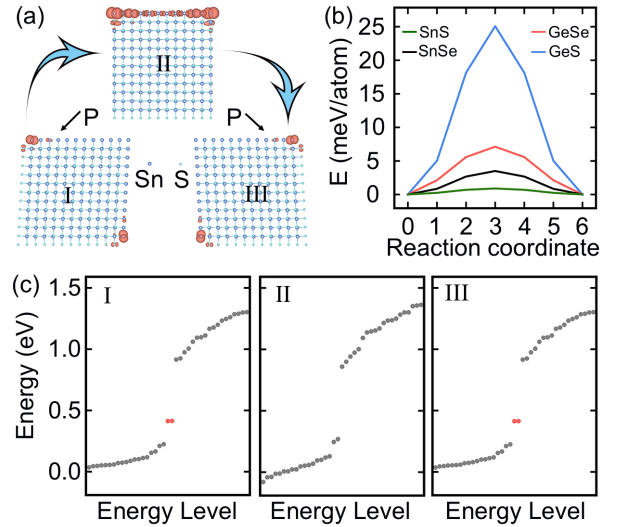


FIG. 5. (a) Distributions of corner states for ferroelastic states I, III, and intermediate state II of SnS. The black arrows for states I and III denote the directions of electric polarization. The green arrows represent for the ferroelastic transition. (b) Energy profile of the kinetic pathway to change the orientations of the electric polarization. (c) Energy spectrum of the SnS nanoflakes under states I, II, and III. Red dots for I and III represent the in-gap corner states.

are clearly visible and electrons are localized mainly at the C_3 -symmetric corners, revealing the higher-order topology of ferroelectric BN bilayers. However, interestingly, six corner states emerge and arise from both the up and down layers for the BA stacking, while there are only three corner states that emerge mainly on the up layer for the AB stacking. This is due to the fact that for BA stacking both the up and down layers are terminated with zigzag edges of B atoms, while, for the AB stacking, the up layer is terminated with zigzag edges of B atoms but the down layer is terminated with armchair edges of N atoms. Besides, with the implementation of an out-of-plane electric field, one can achieve a phase transition between AB and BA stacking. Therefore, the exotic corner states can be controlled to be created and annihilated in different layers.

In fact, all the above realizations of ferroelectric HOTIs are the out-of-plane ferroelectric materials with in-plane quantized polarization, we then seek the realizations in in-plane ferroelectric materials. As intrinsic multiferroic materials, MA ($M = \text{Ge, Sn}; A = \text{S, Se}$) monolayers have been proposed to be coupled with ferroelasticity and ferroelectricity, enabling the nonvolatile memory readable/writable capability at ambient condition [70–72]. As a direct consequence of in-equivalent lattice constants along with the a and b axis, MA have two stable structures, labeled by states I and III, as shown in Fig. 5(a). With the implementation of external in-plane strain or electric field, reversible phase transitions can indeed be obtained between state I-III. By means of the nudged-elastic-band (NEB) method, the overall ferroelastic switching barrier is calculated and presented in Fig. 5(b), almost the same as that of previous theoretical predictions.

To explicitly uncover the HOTI nature, we construct paral-

lelogram nanoflakes of SnS. As shown in Fig. 5(c), two degenerate in-gap states arise around the Fermi level for two ferroelastic states I and III, whereas their accumulation showcase some differences. Effected by polarization, different corners will exhibit different electric potential, rendering an energy splitting between corners. However, the top-left and down-right corners of state I related by the rotation symmetry C_{11} will share an electric potential of the same amplitude. Therefore, the corner states would emerge as a hallmark of HOTI. Similarly, electrons would accumulate in the top-right and down-left corners of state III, preserving the rotation symmetry $C_{1\bar{1}}$. To be contrast, state II presents us edge states for both the top and bottom edges ([see Fig. S4 [57]].) Thus, with the application of strain, one can achieve the transport of corner states, which will give rise to many interesting phenomena and applications.

In conclusion, we have devised a new type of functional phase namely ferroelectric HOTIs and demonstrated that the experimentally synthesized 2D ferroelectrics provide a rich playground to explore. Material candidates are given to traditional ferroelectrics such as In_2S_3 , In_2Se_3 , In_2Te_3 , SnS, GeS, SnSe, GeSe and newly proposed sliding ferroelectrics such as BN, ZnO, AlN, GaN, SiC, InSe, GaSe [57]. We show that the in-plane electric polarizations can give rise to the HOTIs that can be classified into two types with either quantized or non-

quantized polarizations. Remarkably, for all of them, electric fields can be used to control the exotic corner states and induce topological phase transitions. Our studies lay the groundwork for electronically controlled higher-order topological phases, and put forward potential material candidates for exploring the intriguing physics.

DATA AVAILABILITY

The data that support the findings of this study are available from the corresponding author upon reasonable request.

CODE AVAILABILITY

The codes are available from the corresponding author upon reasonable request.

ACKNOWLEDGEMENTS

This work was supported by the National Natural Science Foundation of China (Grants No. 11904205, No. 12074217, and No. 12174220), the Shandong Provincial Natural Science Foundation of China (Grants No. ZR2019QA019 and No. ZR2019MEM013), the Shandong Provincial Key Research and Development Program (Major Scientific and Technological Innovation Project) (Grant No. 2019JZZY010302), and the Qilu Young Scholar Program of Shandong University.

COMPETING INTERESTS

The authors declare no competing interests.

-
- [1] X.-L. Qi, S.-C. Zhang. Topological insulators and superconductors. *Rev. Mod. Phys.* **83**, 1057–1110 (2011).
- [2] M. Hasan, C. Kane. Colloquium: Topological insulators. *Rev. Mod. Phys.* **82**, 3045–3067 (2010).
- [3] A. Bansil, H. Lin, T. Das. Colloquium: Topological band theory. *Rev. Mod. Phys.* **88**, 021004 (2016).
- [4] C. L. Kane, E. J. Mele. Quantum spin Hall effect in graphene. *Phys. Rev. Lett.* **95**, 226801 (2004).
- [5] B. A. Bernevig, T. L. Hughes, S.-C. Zhang. Quantum spin Hall effect and topological phase transition in HgTe quantum wells. *Science* **314**, 1757–1761 (2006).
- [6] C. L. Kane, E. J. Mele. Z_2 topological order and the quantum spin Hall effect. *Phys. Rev. Lett.* **95**, 146802 (2005).
- [7] J. Sinova, S. O. Valenzuela, J. Wunderlich, C. H. Back, T. Jungwirth. Spin hall effects. *Rev. Mod. Phys.* **87**, 1213–1260 (2015).
- [8] W. A. Benalcazar, B. A. Bernevig, T. L. Hughes. Quantized electric multipole insulators. *Science* **357**, 61–66 (2017).
- [9] W. A. Benalcazar, B. A. Bernevig, T. L. Hughes. Electric multipole moments, topological multipole moment pumping, and chiral hinge states in crystalline insulators. *Phys. Rev. B* **96**, 245115 (2017).
- [10] F. Schindler, A. M. Cook, M. G. Vergniory, Z. Wang, S. S. Parkin, B. A. Bernevig, T. Neupert. Higher-order topological insulators. *Sci. Adv.* **4**, eaat0346 (2018).
- [11] N. Mao, H. Wang, Y. Dai, B. Huang, C. Niu. Third-order topological insulators with wallpaper fermions in t14pbte3 and t14snte3. *npj Comput. Mater.* **8**, 1–7 (2022).
- [12] N. Mao, R. Li, Y. Dai, B. Huang, B. Yan, C. Niu. Orbital shift-induced boundary obstructed topological materials with a large energy gap. *arXiv preprint arXiv:2207.02618* (2022).
- [13] Z. Song, T. Zhang, Z. Fang, C. Fang. Quantitative mappings between symmetry and topology in solids. *Nat. Commun.* **9**, 3530 (2018).
- [14] H. C. Po, A. Vishwanath, H. Watanabe. Symmetry-based indicators of band topology in the 230 space groups. *Nat. Commun.* **8**, 1–9 (2017).
- [15] F. Tang, H. C. Po, A. Vishwanath, X. Wan. Topological materials discovery by large-order symmetry indicators. *Sci. Adv.* **5**, eaau8725 (2019).
- [16] M. Ezawa. Topological switch between second-order topological insulators and topological crystalline insulators. *Phys. Rev. Lett.* **121**, 116801 (2018).
- [17] Y. Xu, Z. Song, Z. Wang, H. Weng, X. Dai. Higher-order topology of the axion insulator EuIn_2As_2 . *Phys. Rev. Lett.* **122**, 256402 (2019).
- [18] C. Yue, Y. Xu, Z. Song, H. Weng, Y. M. Lu, C. Fang, X. Dai. Symmetry-enforced chiral hinge states and surface quantum anomalous Hall effect in the magnetic axion insulator $\text{Bi}_{2-x}\text{Sm}_x\text{Se}_3$. *Nat. Phys.* **15**, 577–581 (2019).
- [19] M. J. Park, Y. Kim, G. Y. Cho, S. Lee. Higher-order topological insulator in twisted bilayer graphene. *Phys. Rev. Lett.* **123**, 216803 (2019).
- [20] X.-L. Sheng, C. Chen, H. Liu, Z. Chen, Z.-M. Yu, Y. Zhao, S. A. Yang. Two-dimensional second-order topological insulator in graphdiyne. *Phys. Rev. Lett.* **123**, 256402 (2019).
- [21] B. Liu, G. Zhao, Z. Liu, Z. Wang. Two-dimensional quadrupole topological insulator in γ -graphyne. *Nano Lett.* **19**, 6492–6497 (2019).
- [22] E. Lee, R. Kim, J. Ahn, B.-J. Yang. Two-dimensional higher-order topology in monolayer graphdiyne. *npj Quantum Mater.* **5**, 1–7 (2020).
- [23] C. Chen, Z. Song, J.-Z. Zhao, Z. Chen, Z.-M. Yu, X.-L. Sheng,

- S. A. Yang. Universal approach to magnetic second-order topological insulator. *Phys. Rev. Lett.* **125**, 056402 (2020).
- [24] Y. Ren, Z. Qiao, Q. Niu. Engineering corner states from two-dimensional topological insulators. *Phys. Rev. Lett.* **124**, 166804 (2020).
- [25] F. Schindler, Z. Wang, M. G. Vergniory, A. M. Cook, A. Murani, S. Sengupta, A. Y. Kasumov, R. Deblock, S. Jeon, I. Drozdov, H. Bouchiat, S. Guéron, A. Yazdani, B. A. Bernevig, T. Neupert. Higher-order topology in bismuth. *Nat. Phys.* **14**, 918–924 (2018).
- [26] Y. B. Choi, Y. Xie, C. Z. Chen, J. Park, S. B. Song, J. Yoon, B. J. Kim, T. Taniguchi, K. Watanabe, J. Kim, K. C. Fong, M. N. Ali, K. T. Law, G. H. Lee. Evidence of higher-order topology in multilayer WTe₂ from Josephson coupling through anisotropic hinge states. *Nat. Mater.* **19**, 974–979 (2020).
- [27] R. Noguchi, M. Kobayashi, Z. Jiang, K. Kuroda, T. Takahashi, Z. Xu, D. Lee, M. Hirayama, M. Ochi, T. Shirasawa, et al. Evidence for a higher-order topological insulator in a three-dimensional material built from van der Waals stacking of bismuth-halide chains. *Nat. Mater.* **20**, 473–479 (2021).
- [28] J. Valasek. Piezo-electric and allied phenomena in rochelle salt. *Phys. Rev.* **17**, 475 (1921).
- [29] Z. Guan, H. Hu, X. Shen, P. Xiang, N. Zhong, J. Chu, C. Duan. Recent progress in two-dimensional ferroelectric materials. *Adv. Electron. Mater.* **6**, 1900818 (2020).
- [30] M. Wu. Two-dimensional van der Waals ferroelectrics: Scientific and technological opportunities. *ACS Nano* **15**, 9229–9237 (2021).
- [31] N. A. Spaldin. A beginner's guide to the modern theory of polarization. *J. Solid State Chem* **195**, 2–10 (2012).
- [32] S. Liu, Y. Kim, L. Z. Tan, A. M. Rappe. Strain-induced ferroelectric topological insulator. *Nano Lett.* **16**, 1663–1668 (2016).
- [33] B. Monserrat, J. W. Bennett, K. M. Rabe, D. Vanderbilt. Antiferroelectric topological insulators in orthorhombic amgbi compounds (a= li, na, k). *Phys. Rev. Lett.* **119**, 036802 (2017).
- [34] L. Kou, H. Fu, Y. Ma, B. Yan, T. Liao, A. Du, C. Chen. Two-dimensional ferroelectric topological insulators in functionalized atomically thin bismuth layers. *Phys. Rev. B* **97**, 075429 (2018).
- [35] Z. Fei, W. Zhao, T. A. Palomaki, B. Sun, M. K. Miller, Z. Zhao, J. Yan, X. Xu, D. H. Cobden. Ferroelectric switching of a two-dimensional metal. *Nature* **560**, 336–339 (2018).
- [36] H. Bai, X. Wang, W. Wu, P. He, S. A. Yang, Y. Lu, et al. Nonvolatile ferroelectric control of topological states in two-dimensional heterostructures. *Phys. Rev. B* **102**, 235403 (2020).
- [37] D.-F. Shao, J. Ding, G. Gurung, S.-H. Zhang, E. Y. Tsymbal. Interfacial crystal hall effect reversible by ferroelectric polarization. *Phys. Rev. Appl.* **15**, 024057 (2021).
- [38] J. Huang, X. Duan, S. Jeon, Y. Kim, J. Zhou, J. Li, S. Liu. On-demand quantum spin hall insulators controlled by two-dimensional ferroelectricity. *Mater. Horiz.* **9**, 1440–1447 (2022).
- [39] P. Sharma, F.-X. Xiang, D.-F. Shao, D. Zhang, E. Y. Tsymbal, A. R. Hamilton, J. Seidel. A room-temperature ferroelectric semimetal. *Sci. Adv.* **5**, eaax5080 (2019).
- [40] S. Dong, J.-M. Liu, S.-W. Cheong, Z. Ren. Multiferroic materials and magnetoelectric physics: symmetry, entanglement, excitation, and topology. *Adv. Phys.* **64**, 519–626 (2015).
- [41] S. Dong, J.-M. Liu. Recent progress of multiferroic perovskite manganites. *Mod. Phys. Lett.* **26**, 1230004 (2012).
- [42] X. Qi, J. Zhou, Z. Yue, Z. Gui, L. Li, S. Buddhudu. A ferroelectric ferromagnetic composite material with significant permeability and permittivity. *Adv. Funct. Mater.* **14**, 920–926 (2004).
- [43] N. Sebastián, L. Cmok, R. J. Mandle, M. R. de la Fuente, I. D. Olenik, M. Čopič, A. Mertelj. Ferroelectric-ferroelastic phase transition in a nematic liquid crystal. *Phys. Rev. Lett.* **124**, 037801 (2020).
- [44] X. Liu, A. P. Pyatakov, W. Ren. Magnetoelectric coupling in multiferroic bilayer *vs*₂. *Phys. Rev. Lett.* **125**, 247601 (2020).
- [45] C. Xu, P. Chen, H. Tan, Y. Yang, H. Xiang, L. Bellaiche. Electric-field switching of magnetic topological charge in type-i multiferroics. *Phys. Rev. Lett.* **125**, 037203 (2020).
- [46] V. Garcia, M. Bibes, L. Bocher, S. Valencia, F. Kronast, A. Crassous, X. Moya, S. Enouz-Vedrenne, A. Gloter, D. Imhoff, et al. Ferroelectric control of spin polarization. *Science* **327**, 1106–1110 (2010).
- [47] B. Monserrat, J. W. Bennett, K. M. Rabe, D. Vanderbilt. Antiferroelectric topological insulators in orthorhombic amgbi compounds (a= li, na, k). *Phys. Rev. Lett.* **119**, 036802 (2017).
- [48] Y. Liang, N. Mao, Y. Dai, L. Kou, B. Huang, Y. Ma. Intertwined ferroelectricity and topological state in two-dimensional multilayer. *npj Comput. Mater.* **7**, 1–6 (2021).
- [49] B. Bradlyn, L. Elcoro, J. Cano, M. G. Vergniory, Z. Wang, C. Felser, M. I. Aroyo, B. A. Bernevig. Topological quantum chemistry. *Nature* **547**, 298–305 (2017).
- [50] J. Cano, B. Bradlyn, Z. Wang, L. Elcoro, M. Vergniory, C. Felser, M. Aroyo, B. A. Bernevig. Topology of disconnected elementary band representations. *Phys. Rev. Lett.* **120**, 266401 (2018).
- [51] Y. Xu, L. Elcoro, G. Li, Z.-D. Song, N. Regnault, Q. Yang, Y. Sun, S. Parkin, C. Felser, B. A. Bernevig. Three-dimensional real space invariants, obstructed atomic insulators and a new principle for active catalytic sites. *arXiv:2111.02433* (2021).
- [52] Y. Xu, L. Elcoro, Z.-D. Song, M. Vergniory, C. Felser, S. S. Parkin, N. Regnault, J. L. Mañes, B. A. Bernevig. Filling-enforced obstructed atomic insulators. *arXiv:2106.10276* (2021).
- [53] A. Nelson, T. Neupert, T. c. v. Bzdušek, A. Alexandradinata. Multicellularity of delicate topological insulators. *Phys. Rev. Lett.* **126**, 216404 (2021).
- [54] F. Schindler, B. A. Bernevig. Noncompact atomic insulators. *Phys. Rev. B* **104**, L201114 (2021).
- [55] J. Gao, Y. Qian, H. Jia, Z. Guo, Z. Fang, M. Liu, H. Weng, Z. Wang. Unconventional materials: the mismatch between electronic charge centers and atomic positions. *Sci. Bull.* (2022).
- [56] G. Li, Y. Xu, Z. Song, Q. Yang, Y. Zhang, J. Liu, U. Gupta, V. Süß, Y. Sun, P. Sessi, et al. Obstructed surface states as the descriptor for predicting catalytic active sites in inorganic crystalline materials. *Adv. Mater.* 2201328 (2022).
- [57] See *Supplemental Material for details of other ferroelectric HOTI material candidates*.
- [58] W. A. Benalcazar, T. Li, T. L. Hughes. Quantization of fractional corner charge in C_n -symmetric higher-order topological crystalline insulators. *Phys. Rev. B* **99**, 245151 (2019).
- [59] R. B. Jacobs-Gedrim, M. Shanmugam, N. Jain, C. A. Durcan, M. T. Murphy, T. M. Murray, R. J. Matyi, R. L. Moore, B. Yu. Extraordinary photoresponse in two-dimensional in2se3 nanosheets. *ACS Nano* **8**, 514–521 (2014).
- [60] W. Ding, J. Zhu, Z. Wang, Y. Gao, D. Xiao, Y. Gu, Z. Zhang, W. Zhu. Prediction of intrinsic two-dimensional ferroelectrics in in2se3 and other iii2-vi3 van der Waals materials. *Nat. Commun.* **8**, 1–8 (2017).
- [61] C. Cui, W.-J. Hu, X. Yan, C. Addiego, W. Gao, Y. Wang, Z. Wang, L. Li, Y. Cheng, P. Li, et al. Intercorrelated in-plane and out-of-plane ferroelectricity in ultrathin two-dimensional layered semiconductor in2se3. *Nano Lett.* **18**, 1253–1258 (2018).

- [62] X. Tao, Y. Gu. Crystalline–crystalline phase transformation in two-dimensional In_2Se_3 thin layers. *Nano Lett.* **13**, 3501–3505 (2013).
- [63] L. Ju, X. Tan, X. Mao, Y. Gu, S. Smith, A. Du, Z. Chen, C. Chen, L. Kou. Controllable CO_2 electrocatalytic reduction via ferroelectric switching on single atom anchored In_2Se_3 monolayer. *Nat. Commun.* **12**, 1–10 (2021).
- [64] Z. Zhang, J. Nie, Z. Zhang, Y. Yuan, Y.-S. Fu, W. Zhang. Atomic visualization and switching of ferroelectric order in β - In_2Se_3 films at the single layer limit. *Adv. Mater.* **34**, 2106951 (2022).
- [65] J. Zhou, Q. Zeng, D. Lv, L. Sun, L. Niu, W. Fu, F. Liu, Z. Shen, C. Jin, Z. Liu. Controlled synthesis of high-quality monolayered α - In_2Se_3 via physical vapor deposition. *Nano Lett.* **15**, 6400–6405 (2015).
- [66] Y. Zhou, D. Wu, Y. Zhu, Y. Cho, Q. He, X. Yang, K. Herrera, Z. Chu, Y. Han, M. C. Downer, et al. Out-of-plane piezoelectricity and ferroelectricity in layered α - In_2Se_3 nanoflakes. *Nano Lett.* **17**, 5508–5513 (2017).
- [67] X. Ma, C. Liu, W. Ren, S. A. Nikolaev. Tunable vertical ferroelectricity and domain walls by interlayer sliding in β - ZrI_2 . *npj Comput. Mater.* **7**, 1–9 (2021).
- [68] K. Yasuda, X. Wang, K. Watanabe, T. Taniguchi, P. Jarillo-Herrero. Stacking-engineered ferroelectricity in bilayer boron nitride. *Science* **372**, 1458–1462 (2021).
- [69] L. Li, M. Wu. Binary compound bilayer and multilayer with vertical polarizations: two-dimensional ferroelectrics, multiferroics, and nanogenerators. *ACS Nano* **11**, 6382–6388 (2017).
- [70] M. Wu, X. C. Zeng. Intrinsic ferroelasticity and/or multiferroicity in two-dimensional phosphorene and phosphorene analogues. *Nano Lett.* **16**, 3236–3241 (2016).
- [71] R. Fei, W. Kang, L. Yang. Ferroelectricity and phase transitions in monolayer group-IV monochalcogenides. *Phys. Rev. Lett.* **117**, 097601 (2016).
- [72] N. Higashitarumizu, H. Kawamoto, C.-J. Lee, B.-H. Lin, F.-H. Chu, I. Yonemori, T. Nishimura, K. Wakabayashi, W.-H. Chang, K. Nagashio. Purely in-plane ferroelectricity in monolayer SnS at room temperature. *Nat. Commun.* **11**, 1–9 (2020).